DNA Surface Hybridization: Comparison of Theory and Experiment

Damion Irving,[†] Ping Gong,[‡] and Rastislav Levicky*,[†]

Department of Chemical & Biological Engineering, Polytechnic Institute of New York University, Brooklyn, New York 11201, and Seventh Sense Biosystems, Cambridge, Massachusetts 02142

Received: January 28, 2010; Revised Manuscript Received: April 16, 2010

The design and interpretation of surface hybridization assays is complicated by poorly understood aspects of the interfacial environment that cause both kinetic and thermodynamic behaviors to deviate from those in solution. The origins of these differences lie in the additional interactions experienced by hybridizing strands at the surface. In this report, an analysis of surface hybridization equilibria is provided for end-tethered, single-stranded oligonucleotide "probes" hybridizing with similarly sized, single-stranded solution "target" molecules. Theoretical models by Vainrub and Pettitt (*Phys. Rev. E* **2002**, *66*, 041905) and by Halperin, Buhot, and Zhulina (*Biophys. J.* **2004**, *86*, 718), and an "extended" model that in addition includes a solution-like salt dependence of probe-target dimerization, are compared to experiments as a function of salt concentration and probe coverage. Good agreement with experiment is observed when the DNA volume fraction at the surface remains below ∼0.25. None of the models, however, can account for strong suppression of hybridization when the volume fraction of DNA approaches 0.3, realizable in the limit of high buffer strength and densely tethered films. Under these conditions, hybridization yields become insensitive to increases in analyte concentration even though many probes remain available to bind targets. These observations are attributed to the onset of packing constraints which, interestingly, become limiting significantly below maximum DNA coverages estimated from ideally efficient hexagonal packing. By delineating conditions under which specific hybridization behaviors are observed, the results advance fundamental knowledge in support of DNA microarray and biosensor applications.

1. Introduction

In surface hybridization, analyte "target" strands from solution undergo base-sequence specific binding to nucleic acid "probe" strands immobilized on a solid support. A number of technologies, from DNA microarrays for gene expression[1] to biosensors,[2,3] rely on quantitative measurement of surface hybridization to determine the corresponding solution concentrations. Design and interpretation of surface hybridization experiments is made challenging by the complexity of electrostatic, conformational, and molecular interaction phenomena that arise in the crowded interfacial environment. To clarify the mechanisms that influence surface hybridization a number of studies have focused on kinetic[4−25] as well as thermodynamic[4,6,10,11,14,17,19−22,26−35] aspects of noncompetitive (i.e., single type of target) assays. Some of the questions considered have included the influence of probe coverage,[5,7,8,11,13,14,21,25,29−31,36−39] ionic strength,[4,13,31] probe and target lengths,[4,6,9,12,14,16,20,23,25,29,35,39] and surface chemical treatments.[17,38] An outstanding challenge is to relate experimental observations, such as suppression of equilibrium constants relative to solution,[4,11,14,21,27,31,40] to the causative interactions experienced by the hybridizing molecules. These include interactions between probe sites, between the strands and the solid support, and between targets in solution and the like-charged probe layer.

The present report analyzes how these various contributions distinguish surface from solution hybridization. Experimental data, obtained over a range in probe coverage and ionic strength,[31] are compared to theoretical models including those of Vainrub and Pettitt[32] (VP) and Halperin, Buhot, and Zhulina[34] (HBZ), which emphasize electrostatics of target partitioning into the probe layer, as well as an extended HBZ-type model that in addition includes a solution-like salt-dependence of probe−target dimerization. The models are found to be most successful under conditions when the layers are not too crowded, where a consistent picture arises of the differences between surface and solution hybridization. None of the models, however, can account for strong suppression of hybridization observed under high degrees of crowding, when the volume fraction of DNA exceeds 0.25. Moreover, whereas for lower volume fractions hybridization isotherms approach the Langmuir form, as the layer becomes increasingly crowded the hybridization yield becomes insensitive to target concentration and isotherms become pronouncedly non-Langmuirian. These various observations are interpreted to describe how probe coverage and ionic strength impact surface hybridization under a broad range of conditions encountered in diagnostic applications.

2. Methods

2.1. An Extended Model of Surface Hybridization. In this section, a description of surface hybridization is derived that allows for electrostatic costs of target entry into the probe layer as well as, separately, of target−probe pairing (dimerization) under the conditions prevailing in the layer. The model will be used to analyze recent hybridization data[31] as a function of salt concentration and probe coverage. Following the approach of HBZ,[34] the probe layer is described as a slab with a uniform internal concentration of immobilized charge from the probes and hybridized targets. To correspond to our experimental situation, we account for partitioning of mobile ions of multiple

* To whom correspondence should be addressed. Tel: 718-260-3682. Fax: 718-260-3125. E-mail: rlevicky@poly.edu.
[†] Polytechnic Institute of New York University.
[‡] Seventh Sense Biosystems.

10.1021/jp100860z
Published on Web 05/14/2010

valencies between the buffer and the probe layer and also include an explicit salt-dependence of probe−target dimerization due to participation of counterions in duplex formation. Electrochemical equilibria are used to describe the partitioning of mobile buffer ions (Na^+, $H_2PO_4^-$, HPO_4^{2-}, and PO_4^{3-}) and of target strands. Since the probe layer is nearly electroneutral under conditions that produce significant hybridization, this assumption is used to simplify the derivation. Situations involving long spacers and long targets can bring additional corrections to surface hybridization,[41,42] but will not be needed for our experimental system of short probes and comparable length targets.

In solution, hybridization involves probe−target dimerization as represented by eq 1

$$\mathrm{P} + \mathrm{T} + J\mathrm{I} \leftrightarrow \mathrm{D} \tag{1}$$

where, in addition to P and T strands, formation of duplex D involves association with J counterions I. This association, which is responsible for the salt-dependence of solution hybridization, can be interpreted as reflecting changes in counterion condensation due to hybridization-induced increase in the backbone charge density,[43,44] more generally, the JI term is simply viewed as accounting for all adjustments in counterion organization derived from hybridization. The equilibrium constant K_B is

$$\ln K_B \equiv \ln\left(\frac{C_{D,B}}{C_{P,B}C_{T,B}C_{I,B}^{\ J}}\right) = -\frac{\Delta G_B^{\ o}}{RT} \tag{2}$$

where $C_{j,B}$ is the buffer concentration of species j, $\Delta G_B^{\ o}$ is the standard free energy of hybridization in buffer, R is the gas constant, and T is the absolute temperature.[45] Hybridization equilibria can be equivalently represented by defining $K_B' = C_{D,B}/(C_{P,B}C_{T,B})$ and $\Delta G_B^{o\prime} = \Delta G_B^{\ o} - JRT \ln C_{I,B}$.[46]

If P and T are taken to combine in a pairwise fashion so that more complex structures, such as one T binding across multiple P,[39] are not considered then reaction 1 still applies to surface hybridization and leads to

$$\ln K_S \equiv \ln\left(\frac{S_D}{S_P C_{T,S} C_{I,S}^{\ J_S}}\right) = \frac{-\Delta G_S^{\ o}}{RT} \tag{3}$$

where K_S is the equilibrium constant for surface hybridization, $\Delta G_S^{\ o}$ is the standard free energy of surface hybridization, and S_D and S_P are surface coverages of duplex and unhybridized probe molecules (molecules/area), respectively. Their sum, $S_0 = S_P + S_D$, is the total coverage probes (unhybridized and hybridized) or, equivalently, the total coverage of binding sites. $C_{T,S}$ and $C_{I,S}$ are target and counterion concentrations inside the probe layer that are estimated as discussed below. As for the solution case, J_S represents salt-dependence of dimerization although the number of counterions involved is not necessarily the same as in solution; i.e. in general $J_S \neq J$.

The target and counterion reference states implicit in $\Delta G_S^{\ o}$ are the same as in solution, e.g. ideal solutions at 1 mol L^{-1}. For probes and duplexes, the reference state is the pure immobilized probe or duplex at the total coverage of binding sites S_0 and under salt conditions providing 1 mol L^{-1} counterions. This reference state includes interactions with the surface as well as between sites (e.g., due to probe−probe association) and therefore, unconventionally, is expected to depend on S_0. An alternate choice for P and D reference states would be under conditions where the sites do not interact, and instead explicitly account for site−site interactions through additional, S_0-dependent terms on the right of eq 3. This alternate description was not used because, as discussed in section 3, the experimental dependence of $\Delta G_S^{\ o}$ on probe coverage was weak over most of the S_0 range (cf. PL regime). This weak dependence indicates that interactions between sites (at 1 mol L^{-1} salt) were dominated by effects not sensitive to S_0, enabling them to be folded into $\Delta G_S^{\ o}$ as a constant offset. This simplification is expected to break down should experimental conditions extend to very sparse films, in which neighbor strands can no longer interact, or to very dense films, in which packing constraints are expected (section 3.3). In such situations, it would be necessary to explicitly account for the S_0-dependence of site−site interactions.

Penalties associated with target entry into the probe layer lead to decreased target concentration at the surface, $C_{T,S} < C_{T,B}$. This decrease can be described in terms of partitioning equilibria between the bulk solution and the probe layer which, for a charged species j, require equality of electrochemical potentials,

$$\mu_j^{\ o} + RT \ln(C_{j,S}) + z_j e N_A V_S = \mu_j^{\ o} + RT \ln(C_{j,B}) \tag{4}$$

where V_S is the electric potential (membrane potential[47,48]) inside the probe layer relative to buffer, z_j is the signed valence of species j, e is the electronic charge, and N_A is Avogadro's number. Rearrangement of eq 4 with j corresponding to counterions I leads to

$$\exp(eN_A V_S/RT) = \left(\frac{C_{I,B}}{C_{I,S}}\right)^{1/z_I} \tag{5}$$

and, substituting back into eq 4, to[47]

$$C_{j,S} = C_{j,B}\left(\frac{C_{I,S}}{C_{I,B}}\right)^{z_j/z_I} \tag{6}$$

As discussed below, under conditions for which significant hybridization takes place it is reasonable to view the probe layer as electroneutral except for relatively thin regions at its boundaries. Over the electroneutral portion,

$$-C_{im} + \sum_j (1 - \Phi) z_j C_{j,S} = -C_{im} + \sum_j (1 - \Phi) z_j C_{j,B}\left(\frac{C_{I,S}}{C_{I,B}}\right)^{z_j/z_I} = 0 \tag{7}$$

where C_{im} is the charge concentration from immobilized P and D strands, and the index j ranges over all charged species that partition into the layer. Φ is the combined P and D volume fraction in the layer. The volume exclusion term $(1 - \Phi)$ recognizes that only this fraction is available to the partitioning species. Φ and C_{im} are calculated from

$$\Phi = \frac{\nu_{nt}}{h}(N_P S_P + N_D S_D) \tag{8}$$

$$C_{\mathrm{im}} = \frac{|z_{\mathrm{P}}|S_{\mathrm{P}} + |z_{\mathrm{D}}|S_{\mathrm{D}}}{hN_{\mathrm{A}}} \tag{9}$$

where υ_{nt} is the volume of a nucleotide, N_{P} and N_{D} are the number of nucleotides in probes and duplexes, h is the thickness of the probe layer, and z_{P} and z_{D} are the signed probe and duplex valencies, respectively. As eq 9 implies, following HBZ,[34] the strand charge is taken to be uniformly smeared over the probe layer at the concentration C_{im}. Division by N_{A} in eq 9 implies use of a molar basis also for the ionic concentrations $C_{j,\mathrm{B}}$. Because z_{P} and z_{D} represent effective values reduced to account for counterion condensation (section 2.2), the intralayer concentration $C_{\mathrm{I,S}}$ represents just the remnant mobile (uncondensed) counterions. The valencies are subject to the constraint

$$z_{\mathrm{D}} = z_{\mathrm{T}} + z_{\mathrm{P}} + z_{\mathrm{I}}J_{\mathrm{S}} \tag{10}$$

since the duplex charge must equal the sum of charges of its constituent components. For given experimental buffer concentrations $C_{j,\mathrm{B}}$ and total probe coverage $S_0 = S_{\mathrm{P}} + S_{\mathrm{D}}$, the set of eqs 7, 6, and 3 are simultaneously solved numerically for $C_{\mathrm{I,S}}$, $C_{\mathrm{T,S}}$, and S_{D}.

The assumption of layer electroneutrality in eq 7, and thus the concentrations $C_{\mathrm{I,S}}$ and $C_{\mathrm{T,S}}$ that it predicts, does not apply at the layer−solution and layer−solid boundaries where gradients in potential and ionic concentrations are expected over distances comparable to the electrostatic screening (Debye) length r_{D}. Nevertheless, taking the estimated values of $C_{\mathrm{I,S}}$ and $C_{\mathrm{T,S}}$ to hold throughout the layer will be a good approximation provided the probe layers are sufficiently thick to be nearly electroneutral over most of their width. This will be true if the ratio of r_{D} to the layer thickness h is small, $r_{\mathrm{D}}/h \ll 1$, in which case the gradients in potential and ionic concentrations are excluded from most of the layer. The value of r_{D} depends on buffer strength C_{B},[49] which in the experiments described below ranged from 0.012 to 1 mol L^{-1} of pH 7.0 phosphate buffer. Ninety percent of experimental conditions with detectable hybridization corresponded to a C_{B} of 0.11 mol L^{-1} or higher, i.e. r_{D} of 0.63 nm or less. h is expected to be about ten times this value (section 2.2), yielding $r_{\mathrm{D}}/h \leq 0.1$ so that the assumption of electroneutrality should be reasonable.[50] At lower buffer strengths the assumption worsens, e.g. $r_{\mathrm{D}}/h \approx 1/3$ for $C_{\mathrm{B}} = 0.012$ mol L^{-1}. These lowest C_{B} conditions, however, did not enter into analysis as they did not produce measurable hybridization.

2.2. Parameter Selection. The following parameters were known and fixed: $N_{\mathrm{P}} = 20$, $N_{\mathrm{D}} = 38$, $\upsilon_{\mathrm{nt}} = 0.53$ nm^3, $RT = 2.45$ kJ mol^{-1} ($T = 295$ K), $C_{\mathrm{T,B}} = 100$ nmol L^{-1}, pH = 7.0, and sodium phosphate buffer $\mathrm{p}K_{\mathrm{a1}} = 2.15$, $\mathrm{p}K_{\mathrm{a2}} = 6.87$, and $\mathrm{p}K_{\mathrm{a3}} = 12.3$. N_{D} equals 38 because, in the experiments, 18mer targets were hybridized to 20mer probes. The three $\mathrm{p}K_{\mathrm{a}}$ values and the pH were used to calculate the buffer ionic concentrations $C_{j,\mathrm{B}}$ ($j = \mathrm{Na}^+$, $\mathrm{H_2PO_4}^-$, $\mathrm{HPO_4}^{2-}$, and $\mathrm{PO_4}^{3-}$) from acid−base equilibria and the total phosphate concentration, C_{B}. C_{B} and S_0 were known from experiment.

Several parameters had to be estimated. The layer thickness h was estimated at 6.1 nm, the length of an 18mer DNA−DNA duplex. This selection is motivated by prior work which showed that even at fairly low coverages of 3×10^{12} cm^{-2} and high ionic strengths of 1 mol L^{-1} NaCl, oligonucleotide duplexes extended away from the surface to about 85% of full length,[51] corresponding to an average tilt angle of about 30° relative to the surface normal. Duplex orientation in more crowded films would be expected to be even more perpendicular. A similar average tilt angle (27°) was found in a recent multiduplex simulation of end-tethered DNA on gold.[52] Further unknowns include the total strand valencies z_{D}, z_{T}, and z_{P}, which represent values corrected for association with counterions. Theory predicts that counterion condensation around polyelectrolytes depends on salt concentration: condensation decreases, and hence polyelectrolyte valency increases, with increasing salt.[53−55] Experiments, however, often indicate independence of counterion condensation on salt for reasons that are not entirely clear[56,57] but presumably reflect details of the counterions' local environment.[55] Motivated by such experimental results, strand valencies were treated as effective, salt-independent values. z_{D} and z_{T} were estimated by optimizing agreement between model-predicted and experimentally observed hybridization extents. z_{P} followed from the valency balance, eq 10. In addition to z_{D} and z_{T}, J_{S} and $\Delta G_{\mathrm{S}}^{\mathrm{o}}$ were also optimized as their values were not known a priori.

For initial values of z_{D}, z_{T}, J_{S}, and $\Delta G_{\mathrm{S}}^{\mathrm{o}}$, eqs 3, 6 and 7 were used to calculate S_{D}, $C_{\mathrm{T,S}}$ and $C_{\mathrm{I,S}}$. This was performed for each of W experimental combinations of buffer strength C_{B} and site coverage S_0. The normalized square difference X^2 between calculated (S_{D}) and experimental (S^*_{D}) duplex coverages,

$$X^2 = \frac{1}{W - Z}\sum_{i=1}^{W}\left(\frac{S_{\mathrm{D},i} - S^*_{\mathrm{D},i}}{S^*_{\mathrm{D},i}}\right)^2 \tag{11}$$

was iteratively minimized by adjustment of the $Z = 4$ model parameters. Points with hybridization below detection ($S^*_{\mathrm{D},i} = 0$) were excluded. A FORTRAN routine was used that performed an initial approximate optimization with the Nelder−Mead downhill simplex algorithm, followed by quasi-Newton optimization to more efficiently locate the X minimum.

2.3. Isotherm Measurements. Thiolate-tethered DNA probe layers of the 20mer sequence 5′ $\mathrm{NH_2}$-$(\mathrm{CH_2})_6$-$\mathrm{PO_3}$-TTT TAA ATT CTG CAA GTG AT-$\mathrm{PO_3}$-$(\mathrm{CH_2})_6$-S-Au 3′ were prepared on 3.18 mm diameter gold disk working electrodes (Bioanalytical Systems). The procedure used was as previously described[31] except that 1 mmol L^{-1} mercaptohexanol in 0.33 mol L^{-1} pH 7.0 potassium phosphate buffer, instead of mercaptopropanol in deionized water, was used for surface passivation. Passivation of the electrode blocks adsorption of the DNA bases and thus facilitates probe hybridization with target molecules.[36,51] To enable electrochemical determination of the duplex coverage S_{D}, target strands were conjugated with the redox tag N-hydroxy succinimide ferrocene carboxylic acid (FcCA-NHS) through a 5′ amine. Conjugates were twice purified by linear gradient HPLC (12% to 60% methanol in 100 mmol L^{-1} hexafluoroisopropanol, 4.5 mmol L^{-1} triethylamine, pH 8.0; 0.5 mL min^{-1} spread over 22 min). S_{D} was determined from the total charge required to fully switch the FcCA tags on hybridized targets between reduced and oxidized states, as determined with cyclic voltammetry (CV) and previously described methods.[31,58] The total probe coverage S_0 was determined through calibration measurements in which films were prepared under identical conditions, but with FcCA-labeled probes. CV measurements were performed on a rotating-disk-electrode setup (Bioanalytical Systems) at 1500 rpm and a CH440A workstation (CH Instruments), using a scan rate of 75 V s^{-1} over a potential range from 0 to 0.65 V. In between CV scans the surface potential was maintained at 0 V. All potentials are quoted versus an Ag/AgCl/3 mol L^{-1} NaCl reference. A platinum wire served as the counter electrode. Redox peaks from electroactive labels were

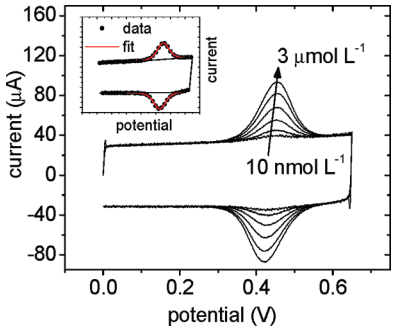

Figure 1. Main panel: Measurement of a hybridization isotherm for $S_0 = 5.0 \times 10^{12}$ cm^{-2}, $C_B = 0.63$ mol L^{-1}, using 9mer targets 5′ CAC TTG CAG 3′. CV traces were taken at increasing concentrations of target from 10 nmol L^{-1} to 3 μmol L^{-1}, after stabilization of hybridization. Inset: An example of a CV fit for $C_{T,B} = 300$ nmol L^{-1}; target coverage was calculated from the area under the fitted peak (red trace) as described previously.[58]

converted to strand coverages by using a custom computer routine.[58] Probe films were maintained wetted under a solution droplet (~50 μL) during all transfers between solutions.

Isotherms were measured in 0.63 mol L^{-1} sodium phosphate buffer deoxygenated by nitrogen bubbling for 1.5 h and filtered through a 0.2 μm filter. Measurements were performed at 22 °C over a 300-fold range in target concentration $C_{T,B}$, from 10 nmol L^{-1} to 3 μmol L^{-1}. Concentrations below 10 nmol L^{-1} were impractical due to equilibration times of hours, while those higher than 3 μmol L^{-1} required overly large quantities of labeled material. An isotherm series was initiated by immersing a freshly prepared probe film working electrode in 10 nmol L^{-1} target solution. CV curves were obtained every 30 min until they stabilized, requiring up to 2.5 h; this end point was taken to represent the equilibrium duplex coverage for that concentration of target. Next, the electrochemical cell was refilled with a fresh target solution of a higher concentration, while keeping the probe film covered by a droplet of solution, and the measurement was repeated at the higher target concentration. Figure 1 shows a set of end point CV traces, one for each target concentration, obtained in this fashion. The FcCA peaks were converted to duplex coverages and used to prepare isotherm plots of S_D vs $C_{T,B}$.

3. Results and Discussion

3.1. Comparison to Experimental Data. Theoretical descriptions of surface hybridization have consistently recognized the role of electrostatics.[32−34] Indeed, experiments show that surface hybridization is sensitive to both salt[4,13,31] and probe coverage.[5,7,8,11,13,14,21,29−31,36−38] Both these dependencies are consistent with the influence of charge. Higher probe coverage S_0 corresponds to greater surface density of negative probes which repel target molecules, and is thus expected to hinder hybridization. A decrease in salt concentration C_B also hinders hybridization, since screening of repulsions between the layer and incoming targets by salt ions becomes weaker.

The above qualitative considerations were first placed on a theoretical footing by Vainrub and Pettitt (VP)[32,59] and subsequently by Halperin, Buhot, and Zhulina (HBZ).[34,60] HBZ derived isotherms for high and low salt conditions. In the more experimentally applicable high salt regime, the functional form of the HBZ isotherm (eqs 9 and 10 of ref 34) can be summarized, together with the VP isotherm (eq 10 of ref 32), by

$$\ln K_S \equiv \ln\left(\frac{S_D}{S_P C_{T,B}}\right) = \frac{-\Delta G_S^{\circ}}{RT} - b_1 r_D^{\,b_2}\sigma_S \qquad (12)$$

$$\sigma_S = |z_P|S_0 + (|z_D| - |z_P|)S_D \qquad (13)$$

where $C_{T,B}$ is the concentration of target in solution, r_D is the Debye length in solution, σ_S is the number of immobilized charges per area including both probe and hybridized target charges, and S_0, S_P, S_D, and ΔG_S° are defined as before. Equation 12 differs from the Langmuir isotherm[61] by the second term on the right, which brings in dependence on salt concentration and surface DNA charge density through r_D and σ_S, respectively. Equations 12 and 13 have four unknown parameters: ΔG_S°, b_2, z_P, and z_D. b_2 was viewed as an unknown because of differing predictions for its value: if the immobilized strand charge distribution is modeled as three-dimensional, as in HBZ, the prediction is $b_2 = 2$.[34] If, as in the earlier model of VP, the layer is viewed as a two-dimensional charged plane then $b_2 = 1$.[32,34] The value of b_1 in eq 12, which acts as a multiplicative factor for the unknowns z_P and z_D and therefore does not provide a separate degree of freedom, was fixed at the theoretical prediction[34] $b_1 = 8\pi|z_T|l_B/h = 32$, obtained using $z_T = -11$ for estimated valency of an 18mer strand corrected for counterion condensation,[43] $l_B = 0.7$ nm for the Bjerrum length l_B in water, and $h = 6.1$ nm for the probe film thickness (section 2.2). Similar to the VP and HBZ theories, the extended model of section 2.1 retains an electrostatic penalty for target partitioning into the probe layer. In the model, this penalty is mediated by the membrane potential V_S, eliciting a cost $z_T e V_S$ for target insertion. In addition, and consistent with hybridization in solution, the extended model specifies a dependence of probe−target dimerization on counterion concentration through J_S. This solution-like salt dependence comes from the direct participation of counterions in hybridization (eq 1) and is retained even if the probe layer becomes so sparse that the penalty to target partitioning is no longer significant.

The theoretical models were compared to earlier experimental data in which the hybridization conversion $x = S_D/S_0$ was determined for 35 combinations of S_0 and sodium phosphate concentration C_B (mol phosphate L^{-1}).[31] Thirteen of the conditions did not yield measurable hybridization, leaving 22 data points for analysis. The experiments used the popular format of mixed monolayers of thiolate-tethered DNA probes and a mercaptoalcohol passivant on gold,[36] with a 20mer probe (5′ TTT TAA ATT CTG CAA GTG AT-$(CH_2)_3$-S-Au 3′), a complementary 18mer target (5′ ATC ACT TGC AGA ATT TAA 3′) present at 100 nmol L^{-1}, and mercaptopropanol passivation of the surface. Hybridization was performed under a surface potential of 0 V vs Ag/AgCl/3 mol L^{-1} NaCl until a stationary duplex coverage S_D was observed for at least 30 min.[31] Although this does not exclude the possibility of further increase over significantly longer times, such measurements are complicated by gradual loss of probe from the surface with the above immobilization method. Up to 12% probe loss was observed during the several hours of measurement.[31]

To better isolate the impact of packing constraints, expected to dominate at high DNA loadings but not accounted for in the models, a series of fits were performed as a function of a volume fraction cutoff Φ_C. This was accomplished by first estimating the DNA volume fraction for each experimental point by using eq 8 and experimental S_P and S_D. Next, each model was fit by using only those points with a volume fraction below Φ_C, $\Phi < \Phi_C$. The analysis started with eight experimental points,

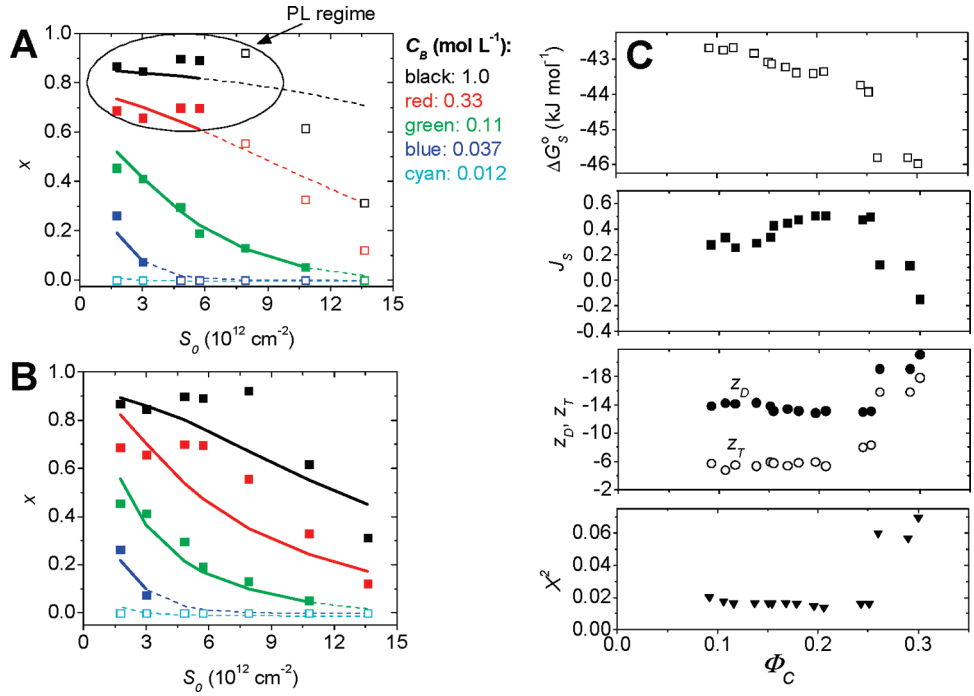

Figure 2. Results using the extended model. Data and fit based on a cutoff of $\Phi_C = 0.2$ (A) and 0.3 (B). Filled symbols: Data used for model fitting. Open symbols: Data excluded from analysis. Solid lines: Predictions of the model over the analyzed conditions. Dotted lines: Extrapolation of model predictions. Conditions corresponding to different buffer concentrations are color-coded. (C) Optimized model parameters ΔG_S^o, J_S, z_D, z_T, and the error X^2, as a function of Φ_C.

corresponding to $\Phi_C = 0.1$, with additional points added sequentially until all 22 points, up to a Φ_C of 0.30, were included. Examples of two such fits are shown in Figure 2, panels A ($\Phi_C = 0.2$) and B ($\Phi_C = 0.3$), using the extended model, where the *y*-axis is the probability (conversion) $x = S_D/S_0$ that a probe site hybridized. In both figures, solid points indicate data for which $\Phi < \Phi_C$; these points were used to derive the best fit indicated by the solid lines. Hollow points indicate experimental data excluded from the model comparison, either because Φ exceeded Φ_C or because no hybridization was observed. Dotted lines indicate how the model predictions, derived from the solid points, extrapolate to conditions represented by the hollow points.

Figure 2C plots the four adjustable parameters of the extended model—ΔG_S^o, J_S, z_D, and z_T—and the corresponding error X^2 as a function of Φ_C. For all four parameters the dependence on Φ_C was modest up to a cutoff of about 0.25 suggesting that, for volume fractions below this value, packing constraints remained weak. However, when Φ_C increased to 0.30 to include the highest coverage data, all parameters exhibited strong shifts accompanied by a pronounced increase in X^2. Examination of panels A and B of Figure 2, which illustrate fits without and with the highest coverage data, reveals these changes can be traced to the model's inability to capture the sharp suppression of hybridization in concentrated buffers ($C_B = 0.33$ and 1.0 mol L^{-1}) as S_0 increases past $\sim 6 \times 10^{12}$ cm^{-2}. This suppression corresponds to the six hollow black and red symbols in Figure 2A. With these points excluded from the analysis, rather good agreement is observed between experiment and calculation as shown by the solid symbols and lines in Figure 2A. In contrast, inclusion of these six points in the analysis leads to a qualitatively worse fit, Figure 2B.

Panels A–C of Figure 3 repeat the above analysis for the VP and HBZ theories, as summarized by eqs 12 and 13. As for the extended model, inclusion of the high coverage data leads to an increase in X^2, indicating that these models are also unable to capture the suppressed hybridization in this limit. Together, these results argue that effects beyond electrostatics, not included in the theories, are responsible for the suppressed hybridization. On the other hand, both the extended model and the isotherm of eq 12 are quite successful in accounting for trends for $\Phi_C < 0.25$, especially at lower salt concentrations where the electrostatic effects included in the models are expected to be prominent. These considerations guide the discussion of the following sections.

3.2. Modestly Crowded Layers ($\Phi < 0.25$). Throughout this section, packing constraints are presumed to be weak so that other effects dominate hybridization. As noted above, electrostatics as described by the models are adequate for capturing experimental trends in the low C_B limit, for buffer strengths of 0.11 mol L^{-1} and below. The situation is more complex at higher buffer concentrations of 0.33 and 1 mol L^{-1}, in the so-called "pseudo-Langmuir" PL regime.[31] Visual comparison of Figures 2A and 3A shows that the extended model was modestly better under PL conditions, with improved separation of the 0.33 and 1 mol L^{-1} curves. This improvement arises from including the salt-dependence of probe–target dimerization via J_S, which more correctly describes variation of K_S with ionic concentration. The models, however, were not able to reproduce the independence of x on S_0 in the PL regime. The fact that such independence is observed experimentally seems to suggest that binding sites do not interact. However, since at these coverages probes must come into contact (see below), PL behavior is perforce interpreted to imply that site–site interactions, while present, do not vary significantly with site coverage. Such invariance may indicate that the interactions are relaxed through structural rearrangements (e.g., changes in strand conformations) as S_0 changes, so that their strength remains approximately constant.

While the models do not explicitly include site–site or strand–surface interactions, they do allow such interactions to

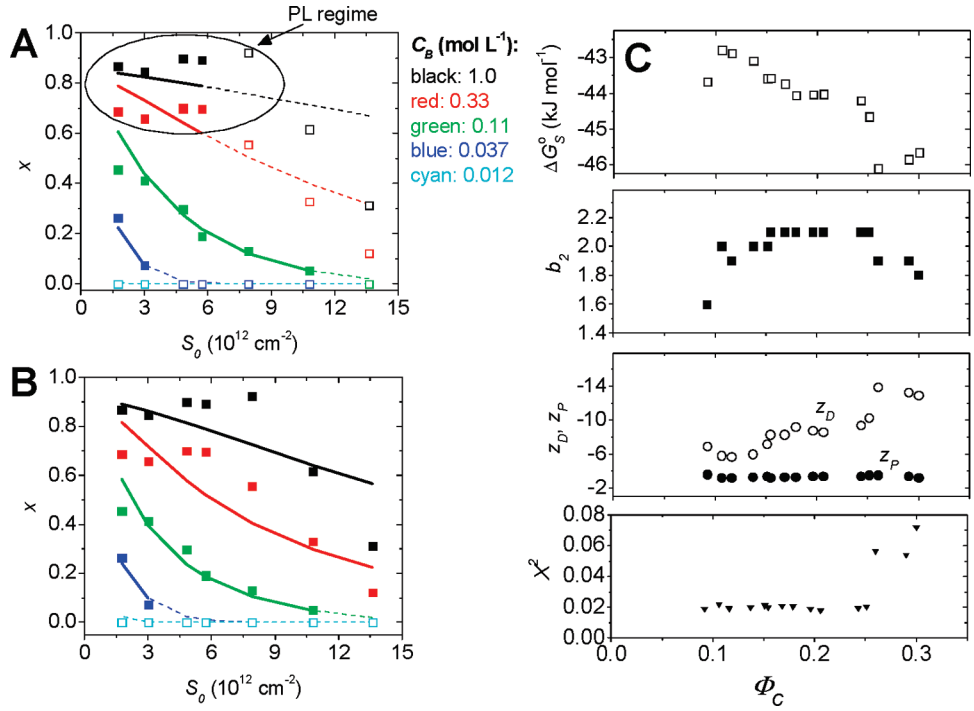

Figure 3. Analysis using the VP and HBZ theories. Data and fit for $\Phi_C = 0.2$ (A) and 0.3 (B). Symbol and line legends are as in Figure 2. (C) Optimized values for ΔG^o_S, b_2, z_D, and z_P as a function of Φ_C, together with the error X^2.

TABLE 1: Optimized Model Parameters for $\Phi_C = 0.2$

parameter	value[a]	benchmark
extended model (section *2.1*)		
ΔG_S^o (kJ mol^{-1})	-43.40 ± 0.25	-101^b
J_S	0.5 ± 0.06	3.1^c
z_D	-12.9 ± 0.4	-10^d
z_T	-6.0 ± 0.8	-11^d
VP and HBZ models (eq *12*)		
ΔG_S^o (kJ mol^{-1})	-44.00 ± 0.35	-101^b
b_2	2.1 ± 0.1	
z_D	-8.8 ± 1.4	-10^d
z_P	-3.4 ± 0.2	

[a] $\pm$ values are variations corresponding to 25% increase in X^2. [b] In solution at 22 °C, 1 mol L^{-1} Na$^+$.[63,75] [c] Derived from eq 7 in ref 46 for solution hybridization. [d] Prediction for an isolated polyelectrolyte in dilute salt.

enter as offsets to ΔG_S^o. From Figure 2C and Table 1, ΔG_S^o is found to be about 60 kJ mol^{-1} less favorable than ΔG^o in solution. That surface hybridization is less favorable indicates stabilization of the unhybridized relative to the duplex state. One plausible mechanism is preference for probe−surface over duplex−surface adsorptive interactions, which is consistent with the observation of remnant strand coverage after films of *un*thiolated single-stranded DNA were treated with a mercaptohexanol displacer.[62] Such experiments indicate that, for at least some surface sites, adsorptive contacts between single-stranded DNA and the surface persist even after passivation. The thermodynamic work required to disrupt such contacts would manifest in a less favorable hybridization free energy, causing an offset in ΔG_S^o relative to solution. In addition, ΔG_S^o must be assumed to be affected by site−site interactions. This is because at the investigated probe coverages, in this as well as other studies,[4,11,14,21,22,27] contacts between neighboring probes and/or duplexes cannot be ruled out. In the present data, the lowest analyzed coverage of $S_0 = 1.8 \times 10^{12}$ cm^{-2} corresponds to an average site separation of 7.5 nm, which is less than the 10 nm contour length of a 20mer probe.

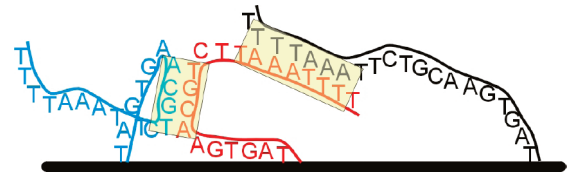

Figure 4. Probe−probe interactions based on regions of highest complementarity. The figure shows the two dominant interactions; other interactions are also possible.

The species most likely to undergo significant interactions are unhybridized probes, rather than duplexes, because of their unpaired bases. In contrast to solution, at the surface interactions between probes are greatly amplified by the high DNA concentration (~0.1 mol L^{-1} nucleotides). For the specific sequence under study, 5′ TTT TAA ATT CTG CAA GTG AT 3′, there are two subsequences of especial interest, illustrated in Figure 4. The first spans from the second to the seventh position at the 5′ end, enabling a TTTAAA/AAATTT probe−probe association. The second spans from the 11th to the 14th position and leads to a TGCA/ACGT interaction. Solution thermodynamics[46,63] predict both interactions to be of comparable strength, with ΔG^o of association between −15 and −20 kJ mol^{-1} (in 1 mol L^{-1} Na$^+$). The positions of the subsequences along the strands, with a 6 or 13 nucleotide linker to the solid support, enable associations throughout the experimental range of site separations from 2.5 to 7.5 nm. These probe−probe interactions can therefore weaken ΔG_S^o by an estimated 30 to 40 kJ mol^{-1}. Interactions involving additional bases outside these sequences are expected to further increase the hybridization penalty; thus, probe−probe interactions could conceivably account for most of the 60 kJ mol^{-1} suppression relative to solution. Consistent with these general notions, a recent multistrand simulation[52] revealed base-stacking and non-Watson−Crick hydrogen bonding between single-stranded regions of surface-tethered DNA oligonucleotides.

Decreased ΔG_S^o values have also been reported for hybridization on nanoparticles,[22,28] and probe−probe associations have been implicated to provide enhanced stability of DNA-modified nanoparticle aggregates.[64] Probe−probe interactions are moreover suspected to be important in microarray measurements. Forman et al. first postulated that probe associations were behind differences in signal saturation for matched and mismatched targets on Affymetrix microarrays.[6] Subsequently, Matveeva et al. analyzed data from Affymetrix and Oxford Gene Technology arrays and found a negative correlation between target hybridization and propensity for interprobe association estimated from solution thermodynamics.[65] Recently, Langdon et al. suggested the existence of multiprobe guanine-guadruplexes based on analysis of data from Affymetrix chips.[66] Interestingly, models of microarray hybridization (e.g., see reviews in refs 67 and 68) based on solution thermodynamics to predict the sequence-dependence of surface hybridization do not explicitly account for probe−probe interactions. In this regard it is significant to note the use of fitting factors in these models to rescale the solution energies; these factors correct for surface effects in a generic sense, including any impact from multiprobe associations.

The next parameter in Table 1, J_S, represents the salt-dependence of probe−target pairing due to reorganization of counterions around the participating strands. Compared to the solution value of $J = 3.1$ estimated from nearest-neighbor models,[46] the surface value is significantly smaller, $J_S \approx 0.5$ (Figure 2C and Table 1). A decrease was already noted in ref 31 where $J_S = 1.1$ was estimated at high ionic strength and low probe coverage, under the assumption that salt-dependence of hybridization is fully attributed to probe−target dimerization (i.e., neglecting electrostatic penalties associated with target partitioning into the probe layer). That J_S is determined to be less than J implies a more modest change in the organization of DNA counterions when hybridization occurs on a surface. A lower J_S would indeed be expected if, as discussed above, association of probes leads to their existence in a partially double-stranded character already prior to hybridization, thus decreasing the net change in amount of double-stranded structure when target binds. Interestingly, studies of DNA hybridization on gold nanoparticles[28] have reported that both the enthalpy and entropy of surface hybridization undergo comparable fractional changes relative to their solution values. This observation is consistent with the pre-existence of double-stranded structure in the probe layer, provided changes in the thermodynamic quantities are linearly proportional to the number of additional base pairs formed by hybridization.

The derived strand valencies $z_D \approx -13$ and $z_T \approx -5.5$ (Figure 2C and Table 1) can be compared to solution values of $z_D \approx -10$ and $z_T \approx -11$ predicted by counterion condensation theory in the limit of dilute salt. This level of agreement is satisfying in view of the simplified representation of the interfacial environment. That z_T is about half its expected solution value may in part reflect compensation for neglect of relaxation mechanisms that would, in the real system, act to decrease the penalty associated with target entry into the probe layer. These mechanisms include a gradual, instead of a step, change in potential from its solution limit to the asymptotic membrane potential V_S; thus, not all charges on a hybridized target will locate so deep in the layer as to experience the limiting V_S value. Also structural adjustments of the layer, such as swelling, will weaken the responsiveness of the potential to variation in S_0 or C_B. Such relaxation mechanisms would decrease costs and sensitivity of target partitioning to S_0 and C_B, and in their absence from the models might lead to compensation through a smaller effective target valency z_T.

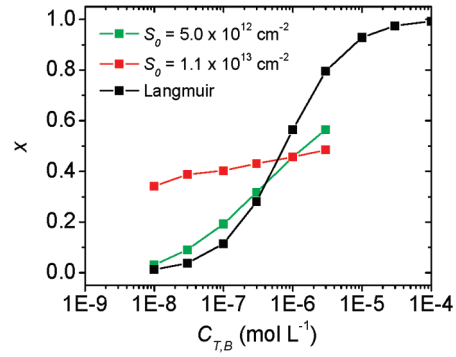

Figure 5. Experimental hybridization isotherms plotting the conversion $x = S_D/S_0$ against target concentration $C_{T,B}$ at moderate ($S_0 = 5.0 \times 10^{12}$ cm^{-2}; green trace) and high ($S_0 = 1.1 \times 10^{13}$ cm^{-2}; red trace) probe coverages, in 0.63 mol L^{-1} pH 7.0 phosphate buffer. A calculated Langmuir isotherm (black trace) is shown for comparison, assuming an affinity constant $K_S = 1.3 \times 10^6$ mol^{-1} L. A different K_S would translate the Langmuir trace horizontally, but not change its shape.

For the analysis based on the isotherm expression 12, the optimized exponent b_2 is found to be close to 2 (Figure 3C). This agrees with the theoretical prediction $b_2 = 2$ of HBZ when the probe layer is modeled as a three-dimensional, homogeneously charged medium and in the experimentally relevant "salt-screening" regime characterized by $r_D/h \ll 1$.[34] As discussed in section 2.1, $r_D/h \ll 1$ is reasonably satisfied for the majority of the experimental conditions. It follows that the weaker exponent $b_2 = 1$ of the VP model, applicable when the layer is conceptualized as a two-dimensional charged plane,[32] under predicts the experimental dependence on C_B. The corresponding duplex and probe valencies, $z_D \approx -8$ and $z_P \approx -3.4$ (Figure 3C), are smaller than expected. As with z_T of the extended model, these lower values may reflect compensation for assumptions that tend to overestimate the costs of target partitioning.

3.3. Highly Crowded Layers ($\Phi > 0.25$). In the previous section, surface hybridization at sufficiently low DNA loadings ($\Phi < 0.25$) could be largely understood through an offset to ΔG_S^o combined with dependence on C_B and S_0 due to electrostatics of (1) target localization at the surface and (2) probe−target dimerization. These ingredients, however, were insufficient to capture the pronounced suppression of hybridization observed at high ionic strengths and high probe coverages. This suppression is evidenced by the six hollow symbols in the $C_B = 0.33$ and 1 mol L^{-1} data sets in Figure 2A. The dashed lines in Figure 2A show how predictions of the extended model extrapolate to this region; it is clear that the combination of electrostatic effects and a free energy offset that worked well for $\Phi_C < 0.25$ cannot capture the strong suppression observed at higher DNA loadings. Before attributing this suppression to packing constraints it is useful to review additional experimental evidence from hybridization isotherms.

Two isotherms are shown in Figure 5, one at moderate and one at high coverage corresponding respectively to $S_0 = 5.0 \times 10^{12}$ and 1.1×10^{13} cm^{-2}. The lower coverage falls under the $\Phi_C < 0.25$ criterion and lies within the PL regime, the higher coverage belongs to $\Phi_C > 0.25$. Both isotherms were measured at $C_B = 0.63$ mol L^{-1}, which was selected to be intermediate between 0.33 and 1 mol L^{-1}. Target concentrations $C_{T,B}$ ranged from 10 nmol L^{-1} to 3 μmol L^{-1}. The high coverage isotherm ($S_0 = 1.1 \times 10^{13}$ cm^{-2}) used the same 18mer target sequence

as in Figures 2 and 3. The moderate coverage isotherm ($S_0 = 5.0 \times 10^{12}$ cm^{-2}) instead used a 9mer target, of sequence 5′ CAC TTG CAG 3′, complementary to positions 10 to 18 from the probes′ 5′ end. This change of target length was necessary to maintain the hybridization transition near the middle of the experimentally accessible window in target concentration. For comparison, Figure 5 also shows an isotherm calculated from the Langmuir form,[61] $x = K_S C_{T,B}/(1 + K_S C_{T,B})$, using $K_S = 1.3 \times 10^6$ mol^{-1} L.

The moderate and high coverage isotherms are informatively different. Where the moderate coverage isotherm deviates modestly from the Langmuir form, the high coverage isotherm is nearly insensitive to target concentration. This surprisingly weak response is observed despite a plentitude of unhybridized probes on the surface. The conclusion from the $S_0 = 1.1 \times 10^{13}$ cm^{-2} isotherm, therefore, is that a large fraction of the probes are not available. We assign this lack of availability to packing constraints, i.e. to scarcity of space in the layer to accommodate the further addition of target molecules.

The intensity of packing constraints depends on the effective volume occupied by a DNA molecule and on the spatial distribution of the probe attachment points. The volume required by a duplex when surrounded by other duplexes should account for the space required to accommodate hydration and electrostatic interactions between duplexes—if duplexes are so close that these interactions become comparable to the free energy of hybridization, double-stranded structure in a probe layer may be disrupted. The electrostatic and hydration repulsion energy ΔG_{DD} between parallel double-stranded DNA molecules, expressed per base pair, has been found to obey[69,70]

$$\Delta G_{DD} = \frac{a l_{bp} \exp(-d/r_H)}{(2d/\pi r_H)^{1/2}} + \frac{b l_{bp} \exp(-d/r_D)}{(2d/\pi r_D)^{1/2}} \quad (14)$$

where d is the interstrand separation, $r_H \approx 0.3$ nm is the characteristic decay length for the hydration interaction, $l_{bp} = 0.34$ nm is the length per base pair, and a and b are constants determined from experiment.[70] Assuming duplexes are distributed in a hexagonal lattice, with each duplex interacting with six neighbors and with 1.0 mol L^{-1} Na^+ as the counterions,[71] ΔG_{DD} becomes comparable to the surface hybridization ΔG_S^o of 2.4 kJ (mol bp)$^{-1}$ for $d = 2.8$ nm. This rough estimate predicts an effective duplex radius of 1.4 nm, corresponding to a maximum hexagonally packed duplex coverage of 1.5×10^{13} cm^{-2}.[72] This predicted coverage significantly exceeds the one observed which, for the high coverage isotherm, is around 4.9×10^{12} cm^{-2}. There are at least two possible causes of the discrepancy. First, the lateral duplex organization is constrained by distribution of the probe attachment points which may not allow realization of the highest efficiency, hexagonally close-packed arrangement. For example, if duplexes instead ordered according to a random sequential adsorption (RSA) process, with a maximal fractional coverage of only 0.547[73,74] compared to 0.907 for hexagonal close-packing, then the maximum realizable coverage would be just $(0.547/0.907)\ 1.5 \times 10^{13}$ cm^{-2} $= 9.0 \times 10^{12}$ cm^{-2}. Worse yet, probe associations (Figure 4) may promote probes to attach near each other during preparation of the layer, and this correlation may further hinder their subsequent hybridization.

In addition to possible constraints imposed by probe tethering, duplexes must coexist with any remnant, unhybridized probes which also occupy space in the layer. Assuming that packing constraints fully dominate hybridization at very high coverages, a limit is expected in which adding one more probe should leave space for one less target. In this scenario, the total strand coverage $S_{TOT} = S_0 + S_D$ should approach a limiting value. Interestingly, replotting the data of Figures 2 and 3 in terms of S_{TOT} suggests, for the 1 mol L^{-1} series, an approach to a maximum strand coverage of 1.8×10^{13} cm^{-2} (Figure 6). This S_{TOT} translates to a fractional surface coverage of 0.56, where the surface footprint of a single strand, a_S, was estimated by using $a_S = a_D/2$ with $a_D = \pi b^2$ the cross-sectional area of double-stranded DNA.[72] That this number is significantly below full coverage is noteworthy. It would also be interesting to compare this value to ones determined for other sequences and layer preparation methods since the fractional coverage achievable by hybridization would be expected to depend on the particular distribution of probe attachment points.

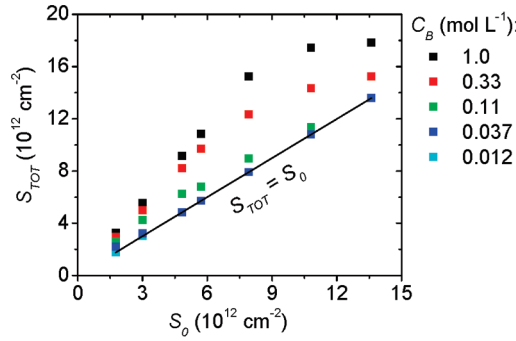

Figure 6. Total strand coverage, S_{TOT}, reached at the end of hybridization as a function of S_0 and C_B. The line $S_{TOT} = S_0$ corresponds to negligible hybridization.

4. Conclusions

Comparison of oligonucleotide surface hybridization experiments with theoretical models over a range in probe coverage ($\sim 1 \times 10^{12}$ to $\sim 1 \times 10^{13}$ cm^{-2}) and buffer strength ($\sim$0.01 to $\sim$1 mol L^{-1}) indicates that, for low to moderately dense layers, thermodynamics of surface hybridization can be understood in terms of two primary corrections relative to solution: (1) electrostatic corrections due to partitioning of targets into the probe layer and due to modified participation of counterions in

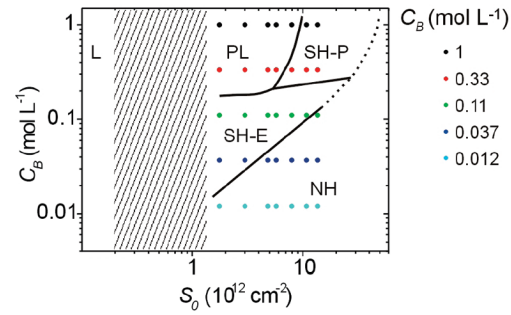

Figure 7. A diagram of hybridization regimes as a function of probe coverage S_0 and buffer strength C_B, for the 18mer target 5′ ATC ACT TGC AGA ATT TAA 3′ binding to end-immobilized 20mer probe 5′ TTT TAA ATT CTG CAA GTG AT 3′. The points represent conditions at which hybridization was measured. The suppressed hybridization (SH) regime has been split into subregimes where suppression is dominated by packing (SH-P) or electrostatic (SH-E) penalties. Dotted lines represent expected boundaries; solid lines are derived from data trends. Hybridization was below detection in the nonhybridizing (NH) regime. The low coverages in the shaded region, culminating in the putative Langmuir regime (L) in which probe sites do not interact, were not experimentally accessible.

probe−target dimerization, and (2) an offset to the standard free energy of hybridization ΔG^{o} attributed to nonelectrostatic interactions (e.g., probe−probe associations) that compete with target binding. The salt-dependence of probe−target dimerization was found to be weaker than in solution, consistent with pre-existence of partial double-stranded character in the layer due to associations between probes. When hybridization occurred under highly crowded conditions, with the surface DNA volume fraction exceeding 25%, enhanced suppression of hybridization observed experimentally could no longer be adequately explained by the models. The suppression was accompanied by insensitivity of hybridization yields to increases in target concentration, despite a plentitude of available probes. These observations were attributed to packing limitations on the allowable surface DNA loading. In view of these considerations, Figure 7 presents a revised version of the hybridization diagram for this system[31] by dividing the suppressed hybridization (SH) regime into regions dominated by suppression due to electrostatic (SH-E) and packing (SH-P) limitations. That packing limitations arose at coverages significantly below those predicted by hexagonal packing suggests the existence of constraints that force duplexes to adopt less efficient packing geometries.

Acknowledgment. This work was supported by the National Science Foundation under Award No. DMR 07-06170, with partial support from DGE-07-41714. The authors are grateful to Professors G. S. Manning and E. Trizac for insightful comments regarding counterion condensation.

References and Notes

(1) Müller, H.-J.; Röder, T. *Microarrays*; Elsevier Academic Press: Burlington, MA, 2006.
(2) Vercoutere, W.; Akeson, M. *Curr. Opin. Chem. Biol.* **2002**, *6*, 816.
(3) Sassolas, A.; Leca-Bouvier, B. D.; Blum, L. J. *Chem. Rev.* **2008**, *108*, 109.
(4) Okahata, Y.; Kawase, M.; Niikura, K.; Ohtake, F.; Furusawa, H.; Ebara, Y. *Anal. Chem.* **1998**, *70*, 1288.
(5) Steel, A. B.; Herne, T. M.; Tarlov, M. J. *Anal. Chem.* **1998**, *70*, 4670.
(6) Forman, J. E.; Walton, I. D.; Stern, D.; Rava, R. P.; Trulson, M. O. *ACS Symp. Ser.* **1998**, *682*, 206.
(7) Henry, M. R.; Stevens, P. W.; Sun, J.; Kelso, D. M. *Anal. Biochem.* **1999**, *276*, 204.
(8) Peterson, A. W.; Heaton, R. J.; Georgiadis, R. M. *Nucleic Acids Res.* **2001**, *29*, 5163.
(9) Stillman, B. A.; Tonkinson, J. L. *Anal. Biochem.* **2001**, *295*, 149.
(10) Riccelli, P. V.; Merante, F.; Leung, K. T.; Bortolin, S.; Zastawny, R. L.; Janeczko, R.; Benight, A. S. *Nucleic Acids Res.* **2001**, *29*, 996.
(11) Peterson, A. W.; Wolf, L. K.; Georgiadis, R. M. *J. Am. Chem. Soc.* **2002**, *124*, 14601.
(12) Su, H.-J.; Surrey, S.; McKenzie, S. E.; Fortina, P.; Graves, D. J. *Electrophoresis* **2002**, *23*, 1551.
(13) Zeng, J.; Almadidy, A.; Watterson, J.; Krull, U. K. *Sens. Actuators, B* **2003**, *90*, 68.
(14) Yu, F.; Yao, D.; Knoll, W. *Nucleic Acids Res.* **2004**, *32*, e75.
(15) Sekar, M. M. A.; Bloch, W.; St John, P. M. *Nucleic Acids Res.* **2005**, *33*, 366.
(16) Tawa, K.; Yao, D. F.; Knoll, W. *Biosens. Bioelectron.* **2005**, *21*, 322.
(17) Wong, E. L. S.; Chow, E.; Gooding, J. J. *Langmuir* **2005**, *21*, 6957.
(18) Gao, Y.; Wolf, L. K.; Georgiadis, R. M. *Nucleic Acids Res.* **2006**, *34*, 3370.
(19) Glazer, M.; Fidanza, J. A.; McGall, G. H.; Trulson, M. O.; Forman, J. E.; Suseno, A.; Frank, C. W. *Anal. Biochem.* **2006**, *358*, 225.
(20) Fiche, J. B.; Buhot, A.; Calemczuk, R.; Livache, T. *Biophys. J.* **2007**, *92*, 935.
(21) Mocanu, D.; Kolesnychenko, A.; Aarts, S.; Dejong, A. T.; Pierik, A.; Coene, W.; Vossenaar, E.; Stapert, H. *Anal. Biochem.* **2008**, *380*, 84.
(22) Chen, C. L.; Wang, W. J.; Ge, J.; Zhao, X. S. *Nucleic Acids Res.* **2009**, *37*, 3756.
(23) Chan, V.; Graves, D. J.; McKenzie, S. E. *Biophys. J.* **1995**, *69*, 2243.
(24) Erickson, D.; Dongqing, L.; Krull, U. J. *Anal. Biochem.* **2003**, *317*, 186.
(25) Hagan, M. F.; Chakraborty, A. K. *J. Chem. Phys.* **2004**, *120*, 4958.
(26) Stevens, P. W.; Henry, M. R.; Kelso, D. M. *Nucleic Acids Res.* **1999**, *27*, 1719.
(27) Nelson, B. P.; Grimsrud, T. E.; Liles, M. R.; Goodman, R. M.; Corn, R. M. *Anal. Chem.* **2001**, *73*, 1.
(28) Xu, J.; Craig, S. L. *J. Am. Chem. Soc.* **2005**, *127*, 13227.
(29) Stachowiak, J. C.; Yue, M.; Castelino, K.; Chakraborty, A.; Majumdar, A. *Langmuir* **2006**, *22*, 263.
(30) Lee, C. Y.; Nguyen, P. C. T.; Grainger, D. W.; Gamble, L. J.; Castner, D. G. *Anal. Chem.* **2007**, *79*, 4390.
(31) Gong, P.; Levicky, R. *Proc. Natl. Acad. Sci. U.S.A.* **2008**, *105*, 5301.
(32) Vainrub, A.; Pettitt, B. M. *Phys. Rev. E* **2002**, *66*, 041905.
(33) Vainrub, A.; Pettitt, B. M. *Biopolymers* **2003**, *68*, 265.
(34) Halperin, A.; Buhot, A.; Zhulina, E. B. *Biophys. J.* **2004**, *86*, 718.
(35) Jayaraman, A.; Hall, C. K.; Genzer, J. *Biophys. J.* **2006**, *91*, 2227.
(36) Herne, T. M.; Tarlov, M. J. *J. Am. Chem. Soc.* **1997**, *119*, 8916.
(37) Shen, G.; Anand, M. F. G.; Levicky, R. *Nucleic Acids Res.* **2004**, *32*, 5973.
(38) Gong, P.; Lee, C.-Y.; Gamble, L. J.; Castner, D. G.; Grainger, D. W. *Anal. Chem.* **2006**, *78*, 3326.
(39) Jayaraman, A.; Hall, C. K.; Genzer, J. *J. Chem. Phys.* **2007**, *127*, 144912.
(40) Levicky, R.; Horgan, A. *Trends Biotechnol.* **2005**, *23*, 143.
(41) Halperin, A.; Buhot, A.; Zhulina, E. *Langmuir* **2006**, *22*, 11290.
(42) Halperin, A.; Buhot, A.; Zhulina, E. B. *Biophys. J.* **2005**, *89*, 796.
(43) Manning, G. S. *Q. Rev. Biophys.* **1978**, *11*, 179.
(44) Record, M. T.; Anderson, C. F.; Lohman, T. M. *Q. Rev. Biophys.* **1978**, *11*, 103.
(45) Bloomfield, V. A.; Crothers, D. M.; Tinoco, I., Jr. *Nucleic Acids - Structures, Properties, and Functions*; University Science Books: Sausalito, CA, 2000; p 497.
(46) SantaLucia, J. *Proc. Natl. Acad. Sci. U.S.A.* **1998**, *95*, 1460.
(47) Donnan, F. G. *J. Membr. Sci.* **1995**, *100*, 45.
(48) Wang, K.; Zangmeister, R. A.; Levicky, R. *J. Am. Chem. Soc.* **2009**, *131*, 318.
(49) $r_D = (\varepsilon\varepsilon_0 kT/2N_A e^2 I_S)^{1/2}$, where $I_S = {}^1/_2(\sum_i z_i^2 C_{i,B})$, $\varepsilon = 80$ is the relative permittivity of water, ε_0 is the permittivity of vacuum, and k is the Boltzmann constant.
(50) Screening at the layer−solid interface is governed by r_D based on the intra-layer, rather than buffer, ionic strength. This local ionic strength is expected to be higher than that in solution due to retention of counterions by the probe layer, even when buffer strength is low. Therefore, the estimates in the text, based on the buffer ionic strength, should be conservative.
(51) Levicky, R.; Herne, T. M.; Tarlov, M. J.; Satija, S. K. *J. Am. Chem. Soc.* **1998**, *120*, 9787.
(52) Lee, O.-S.; Schatz, G. C. *J. Phys. Chem. C* **2009**, *113*, 15941.
(53) Netz, R. R.; Orland, H. *Eur. Phys. J. E: Soft Matter Biol. Phys.* **2003**, *11*, 301.
(54) Tellez, G.; Trizac, E. *J. Stat. Mech.: Theory Exp.* **2006**, P06018.
(55) Manning, G. S. *J. Phys. Chem. B* **2007**, *111*, 8554.
(56) Hoagland, D. A.; Smisek, D. L.; Chen, D. Y. *Electrophoresis* **1996**, *17*, 1151.
(57) Keyser, U. F.; Koeleman, B. N.; van Dorp, S.; Krapf, D.; Smeets, R. M. M.; Lemay, S. G.; Dekker, N. H.; Dekker, C. *Nat. Phys.* **2006**, *2*, 473.
(58) Tercero, N.; Wang, K.; Gong, P.; Levicky, R. *J. Am. Chem. Soc.* **2009**, *131*, 4953.
(59) Vainrub, A.; Pettitt, B. M. *J. Am. Chem. Soc.* **2003**, *125*, 7798.
(60) Halperin, A.; Buhot, A.; Zhulina, E. B. *J. Phys.: Condens. Matter* **2006**, *18*, S463.
(61) Langmuir, I. *J. Am. Chem. Soc.* **1916**, *38*, 2221.
(62) Steel, A. B.; Levicky, R. L.; Herne, T. M.; Tarlov, M. J. *Biophys. J.* **2000**, *79*, 975.
(63) Markham, N. R.; Zuker, M. UNAFold: Software for nucleic acid folding and hybridization. In *Bioinformatics, Vol. II. Structure, Functions and Applications*; Keith, J. M., Ed.; Humana Press: Totowa, NJ, 2008; Vol. 453, p 3.
(64) Hill, H. D.; Hurst, S. J.; Mirkin, C. A. *Nano Lett.* **2009**, *9*, 317.
(65) Matveeva, O. V.; Shabalina, S. A.; Nemtsov, V. A.; Tsodikov, A. D.; Gesteland, R. F.; Atkins, J. F. *Nucleic Acids Res.* **2003**, *31*, 4211.
(66) Langdon, W. B.; Upton, G. J. G.; Harrison, A. P. *Briefings Bioinf.* **2009**, *10*, 259.
(67) Binder, H. *J. Phys.: Condens. Matter* **2006**, *18*, S491.
(68) Burden, C. J.; Pittelkow, Y.; Wilson, S. R. *J. Phys.: Condens. Matter.* **2006**, *18*, 5545.
(69) Strey, H. H.; Parsegian, V. A.; Podgornik, R. *Phys. Rev. Lett.* **1997**, *78*, 895.
(70) Strey, H. H.; Parsegian, V. A.; Podgornik, R. *Phys. Rev. E* **1999**, *59*, 999.

(71) A 0.63 mol L^{-1} sodium phosphate buffer, at a pH of 7.0, has a 1.0 mol L^{-1} concentration of Na^{+}.

(72) The cross-sectional area of a double stranded molecule, for an effective radius of 1.4 nm, is 6.2×10^{-14} cm^2. The maximal duplex surface coverage is then $0.907/(6.2 \times 10^{-14}) = 1.5 \times 10^{13}$ cm^{-2}, where the 0.907 correction factor assumed hexagonal packing.

(73) Feder, J. *J. Theor. Biol.* **1980**, *87*, 237.

(74) Talbot, J.; Tarjus, G.; Van Tassel, P. R.; Viot, P. *Colloids Surf., A* **2000**, *165*, 287.

(75) Markham, N. R.; Zuker, M. *Nucleic Acids Res.* **2005**, *33*, W577.

JP100860Z